Received: 9 January 2022 | Revised: 16 December 2022 | Accepted: 19 January 2023

DOI: 10.1002/gamm.202300004

ORIGINAL PAPER

Application of stable inversion to flexible manipulators modeled by the absolute nodal coordinate formulation

Svenja Drücker | **Robert Seifried**

Institute of Mechanics and Ocean Engineering, Hamburg University of Technology, Hamburg, Germany

Correspondence
Svenja Drücker, Institute of Mechanics and Ocean Engineering, Hamburg University of Technology, Eißendorfer Straße 42, 21073 Hamburg, Germany.
Email: svenja.druecker@tuhh.de

Funding information
German Research Foundation (Deutsche Forschungsgemeinschaft), Grant/Award Number: 362536361

Abstract

Compared to conventional robots, flexible manipulators offer many advantages, such as faster end-effector velocities and less energy consumption. However, their flexible structure can lead to undesired oscillations. Therefore, the applied control strategy should account for these elasticities. A feedforward controller based on an inverse model of the system is an efficient way to improve the performance. However, unstable internal dynamics arise for many common flexible robots and stable inversion must be applied. In this contribution, an approximation of the original stable inversion approach is proposed. The approximation simplifies the problem setup, since the internal dynamics do not need to be derived explicitly for the definition of the boundary conditions. From a practical point of view, this makes the method applicable to more complex systems with many unactuated degrees of freedom. Flexible manipulators modeled by the absolute nodal coordinate formulation (ANCF) are considered as an application example.

KEYWORDS

ANCF, boundary value problem, servo-constraints, stable inversion

1 | INTRODUCTION

The general trend to more efficient machines often results in the design of mechatronic systems with lightweight components. However, undesired oscillations can occur due to reduced stiffness of these flexible structures. Such vibrations cannot be damped directly by the available actuators, since the actuators are usually placed at the robots joints and not on the structure itself. Therefore, the systems are underactuated with more degrees of freedom than independent control inputs. Advanced control strategies are necessary in order to prevent and reduce such oscillations with the available actuators.

Control of flexible robots is still a challenging task due to several reasons. The behavior is highly nonlinear due to large rigid body motion and possibly even nonlinear material properties. A two degree of freedom control structure with feedforward and feedback part is a typical control strategy for such systems, see for example, [20]. The feedforward part is responsible for trajectory tracking, while the feedback part is responsible for disturbance rejection. Often, the feedforward controller is an inverse model of the system. Obtaining inverse models for complex underactuated multibody systems is not straightforward, since classical methods, such as the Byrnes-Isidori normal form [23] are burdensome or

impossible to derive. Moreover, the internal dynamics of common flexible multibody systems are often unstable and must be taken care of. One approach redefines the system output to yield stable internal dynamics for the new output [18,22]. It is also proposed to change system parameters such as mass or moment of inertia to yield stable dynamics [19,26]. Alternatively, stable inversion is proposed in [8,10] to obtain a bounded solution to the inverse model problem for the original nonminimum phase system. The stable inversion involves solving a two-point boundary value problem (BVP) for the internal dynamics, which need to be derived explicitly as ordinary differential equations (ODEs) from the equations of motion. The imposed boundaries are based on the stable and unstable manifolds of the zero dynamics. The obtained system input is noncausal, in the sense that the system input starts to manipulate the system before the actual start of the desired trajectory. In order to avoid the pre- and postactuation phase, a modification of the boundary value problem is proposed in [14]. In [6] is shown that the stable inversion is directly possible for an inverse model described by the servo-constraints framework. The servo-constraints framework is introduced in [5] for underactuated multibody systems yielding a set of differential-algebraic equations (DAEs). In order to avoid deriving and imposing boundary conditions altogether, it was shown in [1] that a similar solution is obtained by solving an optimal control problem. This optimal control problem can be posed either in terms of the explicit internal dynamics in ODE form or in the servo-constraints framework. A first comparison of the boundary value problem approach with the optimal control problem is performed in [2], where it is proven that the solution of the optimal control problem converges to the solution of the boundary value problem as pre- and postactuation time goes to infinity. The methodology is applied to several flexible multibody systems in [16].

Most of the systems considered in the context of stable inversion have few unactuated degrees of freedom. The manipulator considered in [2] has one passive joint, while the manipulators in [1,9,26] have two passive joints. For extremely light and flexible systems, models with few unactuated degrees of freedom might not be sufficient. Then, more involved mechanical models, such as finite element approaches, are necessary to accurately reflect the large deformations.

Classical nonlinear finite elements can describe large nonlinear deformations accurately. However, typical elements cannot exactly reproduce large rigid body rotations [29]. The floating frame of reference approach describes large nonlinear motion of a body-related reference frame. Small linear-elastic deformations are considered with respect to the reference frame [25]. In the context of stable inversion, elastic manipulators are considered in [7] and [27] with six and 18 unactuated elastic degrees of freedom, respectively. However, it is not possible with the floating frame of reference approach to efficiently consider large nonlinear deformations. In contrast, the absolute nodal coordinate formulation (ANCF) is proposed in [28] to accurately model large nonlinear deformations and rotations. The ANCF is applied to describe the motion of cables, flexible pendulums [12], rubber chains [17] and tyres [32]. It has also been applied to model flexible manipulators [33,34]. However, due to the model complexity and the difficulties in explicitly deriving its internal dynamics, ANCF beams have not yet been considered in the context of stable inversion.

An alternative approach is taken in [31] to solve the inverse dynamics problem based on servo-constraints for geometrically exact strings. Thereby, the numerical solution is based on a simultaneous space-time discretization, which avoids numerical difficulties, such as an increasing differentiation index of the underlying DAEs.

In this work, the stable inversion problem is considered for highly flexible manipulators. Thereby, the inverse model is described in the servo-constraints framework [5]. An approximation of the original stable inversion problem is proposed. This approximation makes it possible to apply stable inversion to more complex systems than considered so far because an explicit derivation of the internal dynamics is avoided. It is demonstrated for a simple system with one passive joint that the solution with the proposed approximation converges to the solution of the original problem formulation. Afterwards, the methodology is applied to a flexible manipulator modeled by the ANCF for which the original formulation is not applicable.

The structure of the paper is as follows. The underlying multibody model and its inverse dynamics are described in Section 2. Stable inversion and the proposed approximation are introduced in Section 3. A convergence result supports the proposed approximation. Simulation results for a flexible manipulator modeled by the ANCF are shown in Section 4. A summary and conclusion is given in Section 5.

2 | FORWARD AND INVERSE MODEL

The underlying multibody model and the framework of servo-constraints for the computation of the inverse model are introduced in the following. Holonomic underactuated systems are considered with more degrees of freedom than independent control inputs, since they naturally arise for flexible manipulators.

2.1 | Multibody dynamics

There exist different formulations to derive the equations of motion of general multibody systems, see for example, [24]. The application of servo-constraints is independent of the specific modeling approach. Here, systems with f degrees of freedom, and possibly n_c geometric constraints, for example, arising from joints or kinematic loops are considered. In a very general form, the equations of motion can be written as

$$\dot{\boldsymbol{y}} = \boldsymbol{Z}(\boldsymbol{y})\boldsymbol{v}, \tag{1}$$

$$\boldsymbol{M}(\boldsymbol{y},t)\,\dot{\boldsymbol{v}} + \boldsymbol{k}(\boldsymbol{y},\boldsymbol{v},t) = \boldsymbol{q}(\boldsymbol{y},\boldsymbol{v},t) + \boldsymbol{C}(\boldsymbol{y},\boldsymbol{v},t)^{\mathrm{T}}\lambda + \boldsymbol{B}(\boldsymbol{y})\,\boldsymbol{u}, \tag{2}$$

$$\boldsymbol{c}(\boldsymbol{y},\boldsymbol{v},t) = \boldsymbol{0}. \tag{3}$$

Thereby, $\boldsymbol{y} \in \mathbb{R}^n$ are either redundant or generalized coordinates. The matrix $\boldsymbol{Z} \in \mathbb{R}^{n\times n}$ describes the kinematic relationship between the generalized positions $\boldsymbol{y}$ and velocities $\boldsymbol{v} \in \mathbb{R}^n$, $\boldsymbol{M} \in \mathbb{R}^{n\times n}$ denotes the mass matrix, $\boldsymbol{k} \in \mathbb{R}^n$ denotes the Coriolis and centrifugal forces, $\boldsymbol{q} \in \mathbb{R}^n$ describes the applied forces acting on the system and $\boldsymbol{B} \in \mathbb{R}^{n\times m}$ distributes the control input $\boldsymbol{u} \in \mathbb{R}^m$ [24]. Equation (3) describes implicit constraints $\boldsymbol{c} \in \mathbb{R}^{n_c}$. Therefore, the system has $f = n - n_c$ degrees of freedom. In the case of redundant coordinates, these constraints arise from the joints. In the case of generalized coordinates, the constraints usually only occur if systems with kinematic loops are considered. The constraints are enforced by the Lagrange multipliers $\lambda \in \mathbb{R}^{n_c}$ which are distributed by the Jacobian $\boldsymbol{C} \in \mathbb{R}^{n_c\times\, n}$ of the constraints $\boldsymbol{c}$. The system output $\boldsymbol{z} \in \mathbb{R}^m$ is often chosen as the end-effector position and is defined as

$$\boldsymbol{z} = \boldsymbol{h}(\boldsymbol{y}). \tag{4}$$

2.2 | Inverse dynamics

The framework of servo-constraints is applied to compute the inverse model [5,11]. For this purpose, the equations of motion (1)–(3) are appended by the servo-constraints

$$\boldsymbol{s}(\boldsymbol{y},t) = \boldsymbol{h}(\boldsymbol{y}) - \boldsymbol{z}_{\mathrm{d}}(t) = \boldsymbol{0}, \tag{5}$$

which enforce the system output $\boldsymbol{z}$ to equal the sufficiently smooth desired trajectory $\boldsymbol{z}_{\mathrm{d}}$. The resulting differential-algebraic equations

$$\dot{\boldsymbol{y}} = \boldsymbol{Z}(\boldsymbol{y})\boldsymbol{v}, \tag{6}$$

$$\boldsymbol{M}(\boldsymbol{y},t)\,\dot{\boldsymbol{v}} + \boldsymbol{k}(\boldsymbol{y},\boldsymbol{v},t) = \boldsymbol{q}(\boldsymbol{y},\boldsymbol{v},t) + \boldsymbol{C}(\boldsymbol{y},\boldsymbol{v},t)^{\mathrm{T}}\lambda + \boldsymbol{B}(\boldsymbol{y})\,\boldsymbol{u}, \tag{7}$$

$$\boldsymbol{c}(\boldsymbol{y},\boldsymbol{v},t) = \boldsymbol{0}, \tag{8}$$

$$\boldsymbol{s}(\boldsymbol{y},t) = \boldsymbol{h}(\boldsymbol{y}) - \boldsymbol{z}_{\mathrm{d}}(t) = \boldsymbol{0} \tag{9}$$

describe the inverse model. The solution of Equations (6)–(9) includes the control input $\boldsymbol{u}$, which can be directly used as feedforward control $\boldsymbol{u}_{\mathrm{ffw}}$. For minimum phase systems (i.e., stable internal dynamics), the DAEs (6)–(9) can be integrated forward in time by suitable DAE solvers, see for example, [15]. For nonminimum phase systems, the internal dynamics would become unbounded and stable inversion must be applied [8,23].

3 | STABLE INVERSION

For nonminimum phase systems, the inverse model problem (6)–(9) cannot be solved by forward time integration and stable inversion must be applied. This is the case for many flexible manipulators during end-effector tracking. Stable

inversion is proposed in [8] to compute a bounded solution for the inverse model problem. It is formulated for the explicitly stated internal dynamics. The approach is extended to inverse models described by servo-constraints in [6]. Experimental results of the concept are shown in [7,20] for a flexible manipulator. In the following, stable inversion is briefly reviewed and an approximation of the original boundary conditions is proposed. A convergence analysis for a manipulator with one passive joint supports the proposed approximation.

3.1 | Original formulation

For the derivation of the original stable inversion problem, the equations of motion (1)–(2) are considered for multibody systems in minimal coordinates without any geometric constraints ($n_c = 0$). Then, the equations of motion can be summarized for notational simplicity in the input affine form

$$\begin{aligned} \dot{\boldsymbol{x}} &= \boldsymbol{f}(\boldsymbol{x}) + \sum_{i=1}^{m} g_i(\boldsymbol{x})\, u_i, \\ z_1 &= h_1(\boldsymbol{x}), \\ &\vdots \\ z_m &= h_m(\boldsymbol{x}) \end{aligned} \tag{10}$$

with the states $\boldsymbol{x} = \begin{bmatrix} \boldsymbol{y}^{\mathrm{T}} & \boldsymbol{v}^{\mathrm{T}} \end{bmatrix}^{\mathrm{T}}$ and with m inputs u_i and m outputs z_i. The relative degree of a system described by equation (10) is the nonlinear extension to the concept of pole excess of linear systems. It is a property of the system dynamics as well as the chosen system output. For the considered multiinput multioutput systems, the vector relative degree $\boldsymbol{r} = \{r_1, r_2, \ldots, r_m\}$ is considered. It is defined by the number of Lie derivatives taken of each system output z_i with $i = 1, 2, \ldots, m$, until at least one system input appears explicitly. This is described mathematically as

$$z_i^{(k)} = L_{\boldsymbol{f}}^{k}\, h_i(\boldsymbol{x}) + \sum_{j=1}^{m} \underbrace{L_{g_j} L_{\boldsymbol{f}}^{k-1} h_i(\boldsymbol{x})}_{=0}\, u_j = L_{\boldsymbol{f}}^{k}\, h_i(\boldsymbol{x}), \quad 0 \le k \le r_i - 1, \tag{11}$$

$$z_i^{(r_i)} = L_{\boldsymbol{f}}^{r_i} h_i(\boldsymbol{x}) + \sum_{j=1}^{m} \underbrace{L_{g_j} L_{\boldsymbol{f}}^{r_i-1} h_i(\boldsymbol{x})}_{\neq 0}\, u_j, \tag{12}$$

for $i = 1, \ldots, m$. Moreover, the coupling matrix between the input and output channels must be regular, refer to [23,30] for details. In order to extract the internal dynamics explicitly, a nonlinear coordinate transformation is performed. For this purpose, the outputs z_i and their first r_i Lie derivatives are chosen as new coordinates. Since the sum of the entries of the vector relative degree $r = \sum_{j=1}^{m} r_j$ is not necessarily equal to the number of states $2f$, a number of $2f - r$ coordinates must be chosen such that the coordinate transformation is at least a local diffeomorphism. These additional coordinates are called $\boldsymbol{\eta} \in \mathbb{R}^{2f-r}$ and describe the internal dynamics. Performing the coordinate transformation to the system (10) determines the internal dynamics

$$\dot{\boldsymbol{\eta}} = \boldsymbol{\rho}\left(\boldsymbol{z}, \dot{\boldsymbol{z}}, \ldots, \boldsymbol{z}^{(\max(r_i))}, \boldsymbol{\eta}\right). \tag{13}$$

The internal dynamics is driven by the output trajectory $\boldsymbol{z}$. Stability analysis of the nonlinear internal dynamics is usually difficult and is therefore performed for the zero dynamics, defined by zeroing the output with $\boldsymbol{z} = \boldsymbol{0}$ and all its derivatives [23,30]. Then, the zero dynamics is

$$\dot{\boldsymbol{\eta}} = \boldsymbol{\rho}\left(\boldsymbol{0}, \boldsymbol{0}, \ldots, \boldsymbol{0}, \boldsymbol{\eta}\right). \tag{14}$$

which can be linearized around the equilibrium $\boldsymbol{\eta}_{\mathrm{eq}}$. It is assumed that the zero dynamics has an hyperbolic equilibrium point with n^{s} eigenvalues with negative real part and n^{u} eigenvalues positive real part. Details for the derivation of the internal dynamics can be found in [23,30] for general nonlinear systems, in [27] for multibody systems in ODE form and in [3] for nonlinear DAEs.

The stable inversion approach is stated originally for internal dynamics in the form (13). In order to compute a bounded solution of the internal dynamics, boundary conditions are defined such that the initial state starts on the unstable manifold of the equilibrium point and the final state reaches the equilibrium on the stable manifold. Thereby, the stable and unstable manifolds are locally approximated by the stable and unstable eigenspaces of the linearized zero dynamics. The boundary conditions are then given as

$$\boldsymbol{B}_{\mathrm{u}}^{\mathrm{ode}} \left(\boldsymbol{\eta}(T_0) - \boldsymbol{\eta}_{\mathrm{eq}} \right) = 0, \tag{15}$$

$$\boldsymbol{B}_{\mathrm{s}}^{\mathrm{ode}} \left(\boldsymbol{\eta}(T_{\mathrm{f}}) - \boldsymbol{\eta}_{\mathrm{eq}} \right) = 0 \, . \tag{16}$$

Thereby, T_0 and T_{f} denote the initial and final simulation time and $\boldsymbol{\eta}_{\mathrm{eq}}$ is the equilibrium. The matrices $\boldsymbol{B}_{\mathrm{s}}^{\mathrm{ode}} \in \mathbb{R}^{n^{\mathrm{s}} \times (2f-r)}$ and $\boldsymbol{B}_{\mathrm{u}}^{\mathrm{ode}} \in \mathbb{R}^{n^{\mathrm{u}} \times (2f-r)}$ contain the eigenvectors associated with the n^{s} stable and n^{u} unstable eigenvalues of the zero dynamics respectively, see for example, [6] for a detailed derivation of the respective matrices. The solution of the boundary value problem is noncausal, in the sense that the control input $\boldsymbol{u}_{\mathrm{ffw}}$ induces motion before the start of the trajectory at time t_0, which is called preactuation. Moreover, a postactuation is necessary in order to bring the internal dynamics to rest after the end of the trajectory at time t_{f}. Therefore, the simulation time interval $[T_0, \ T_{\mathrm{f}}]$ is chosen larger than the interval $[t_0, \ t_{\mathrm{f}}]$ of the desired trajectory. It holds $T_0 \leq t_0$ and $T_{\mathrm{f}} \geq t_{\mathrm{f}}$.

A similar boundary value problem can be formulated directly for the inverse model (6)–(9) described by servo-constraints [6]. The boundary conditions (15)–(16) are then chosen accordingly for the complete vector of unknowns of the inverse model problem as

$$\boldsymbol{B}_{\mathrm{u}}^{\mathrm{dae}} \left(\boldsymbol{x}(T_0) - \boldsymbol{x}_{\mathrm{eq}} \right) = 0, \tag{17}$$

$$\boldsymbol{B}_{\mathrm{s}}^{\mathrm{dae}} \left(\boldsymbol{x}(T_{\mathrm{f}}) - \boldsymbol{x}_{\mathrm{eq}} \right) = 0. \tag{18}$$

with the matrices $\boldsymbol{B}_{\mathrm{s}}^{\mathrm{dae}} \in \mathbb{R}^{n^{\mathrm{s}} \times (2n+n_{\mathrm{c}}+m)}$ and $\boldsymbol{B}_{\mathrm{u}}^{\mathrm{dae}} \in \mathbb{R}^{n^{\mathrm{u}} \times (2n+n_{\mathrm{c}}+m)}$ and with $\boldsymbol{x}$ collecting all unknown variables $\boldsymbol{x} = \begin{bmatrix} \boldsymbol{y}^{\mathrm{T}} & \boldsymbol{v}^{\mathrm{T}} & \boldsymbol{\lambda}^{\mathrm{T}} & \boldsymbol{u}^{\mathrm{T}} \end{bmatrix}^{\mathrm{T}}$ of the inverse model DAEs (6)–(9).

The derivation of the boundary conditions (15)–(16) or (17)–(18) is not straightforward for general nonlinear multibody systems, since they depend on the internal dynamics. This limits the application of the approach to systems with few degrees of freedom, for which the internal dynamics can be derived explicitly.

3.2 | Approximation of boundary conditions

An approximation of the boundary conditions (15)–(16) or (17)–(18) is proposed in the following. Instead of enforcing the state vector to lie on the stable and unstable manifolds, part of the state vector is directly constrained onto the equilibrium point. For the explicitly given internal dynamics (13) the approximating boundary conditions are of the form

$$\boldsymbol{L}_0^{\mathrm{ode}} \, \boldsymbol{\eta}(T_0) = \boldsymbol{L}_0^{\mathrm{ode}} \, \boldsymbol{\eta}_{\mathrm{eq}} \tag{19}$$

$$\boldsymbol{L}_{\mathrm{f}}^{\mathrm{ode}} \, \boldsymbol{\eta}(T_{\mathrm{f}}) = \boldsymbol{L}_{\mathrm{f}}^{\mathrm{ode}} \, \boldsymbol{\eta}_{\mathrm{eq}} \tag{20}$$

with the binary matrices $\boldsymbol{L}_0^{\mathrm{ode}} \in \mathbb{R}^{n^{\mathrm{a}} \times (2f-r)}$ and $\boldsymbol{L}_{\mathrm{f}}^{\mathrm{ode}} \in \mathbb{R}^{n^{\mathrm{b}} \times (2f-r)}$ selecting n^{a} states to be equal to the equilibrium $\boldsymbol{\eta}_{\mathrm{eq}}$ at time T_0 and n^{b} states to be equal to the equilibrium at time T_{f}. Thereby it is $n^{\mathrm{b}}, n^{\mathrm{a}} > 0$. In total, a number of $n^{\mathrm{a}} + n^{\mathrm{b}} = 2f - r$ conditions are given, which equals the number of unknowns.

Equivalently for the inverse model described by the servo-constraints DAEs (6)–(9), the approximating boundary conditions are proposed as

$$\boldsymbol{L}_0^{\mathrm{dae}} \, \boldsymbol{x}(T_0) = \boldsymbol{L}_0^{\mathrm{dae}} \, \boldsymbol{x}_{\mathrm{eq}} \tag{21}$$

$$\boldsymbol{L}_{\mathrm{f}}^{\mathrm{dae}} \, \boldsymbol{x}(T_{\mathrm{f}}) = \boldsymbol{L}_{\mathrm{f}}^{\mathrm{dae}} \, \boldsymbol{x}_{\mathrm{eq}} \tag{22}$$

with the binary matrices $\boldsymbol{L}_0^{\text{dae}} \in \mathbb{R}^{n^{\text{a}} \times (2n+n_{\text{c}}+m)}$ and $\boldsymbol{L}_{\text{f}}^{\text{dae}} \in \mathbb{R}^{n^{\text{b}} \times (2n+n_{\text{c}}+m)}$ again selecting $n^{\text{a}} > 0$ states to be equal to the equilibrium $\boldsymbol{\eta}_{\text{eq}}$ at time T_0 and $n^{\text{b}} > 0$ states to be equal to the equilibrium at time T_{f}. The number of boundary conditions again equals the number of unknowns with $n^{\text{a}} + n^{\text{b}} = 2n + n_{\text{c}} + m$.

The proposed simplified boundary conditions (19)–(20) and (21)–(22) approximate the correct boundary conditions for small values of the state vectors $\boldsymbol{\eta}$ and $\boldsymbol{x}$ respectively. The approximation reduces the effort for system analysis and makes stable inversion applicable for complex multibody systems.

3.3 | Convergence of approximated BVP

Convergence of the proposed approximation is here shown graphically for a robot with one passive joint. The robot model is shown in Figure 1. It consists of two links, which are connected by a linear spring-damper combination. The minimal coordinates are chosen as α describing the angle of the first link and β describing the angle of the second link relative to the first link. The system input is a torque applied on the first joint, while the system output z is the angle between end-effector and the horizontal line. The simulation parameters are given in Table 1. The internal dynamics of the system can be described by the coordinate β of the passive joint and it can be derived analytically, see [26] for detailed derivations. Here, the analytical solution for the internal dynamics is used to compute a reference solution of the stable inversion approach based on the original boundary conditions. The internal dynamics of the robot is unstable for a homogeneous mass distribution and the output considered here. Therefore, stable inversion with the original boundary conditions as well as with the approximated boundary conditions is applied to compute the feedforward control input in the following. The boundary value problems are solved using finite differences with Simpson discretization.

The desired output trajectory z_{d} is chosen as smooth transition from $z(t_0) = z_0 = 0\,^\circ$ to $z(t_{\text{f}}) = z_{\text{f}} = 30\,^\circ$ defined by

$$z_{\text{d}}(t) = y_0 + (y_{\text{f}} - y_0)\left(126\left(\frac{t}{t_{\text{f}}}\right)^5 - 420\left(\frac{t}{t_{\text{f}}}\right)^6 + 540\left(\frac{t}{t_{\text{f}}}\right)^7 - 315\left(\frac{t}{t_{\text{f}}}\right)^8 + 70\left(\frac{t}{t_{\text{f}}}\right)^9\right), \tag{23}$$

The initial and final time are chosen as $t_0 = 0\,\text{s}$ and $t_{\text{f}} = 1\,\text{s}$. The desired trajectory is shown in Figure 2A. The system input computed by the original stable inversion approach is shown in Figure 2B. It can be seen that there exists a preactuation phase before t_0. This is necessary to obtain a bounded solution for the internal dynamics. The phase space is shown in Figure 2C. It can be seen that the state trajectory leaves the equilibrium in the direction of the unstable eigenspace, denoted by E_0^{u} and reaches the equilibrium in the direction of the stable eigenspace, denoted by E_{f}^{s}, as it is enforced by the boundary conditions.

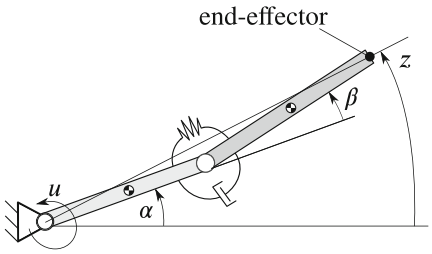

FIGURE 1 Model of a manipulator with one passive joint.

TABLE 1 Simulation parameters of the manipulator with one passive joint.

Parameter	Value
$L_1 = L_2$	0.5 m
$m_1 = m_2$	0.05 kg
d	$2.5 \times 10^{-5}\,\frac{\text{N m s}}{\text{rad}}$
k	$0.5\,\frac{\text{N m}}{\text{rad}}$

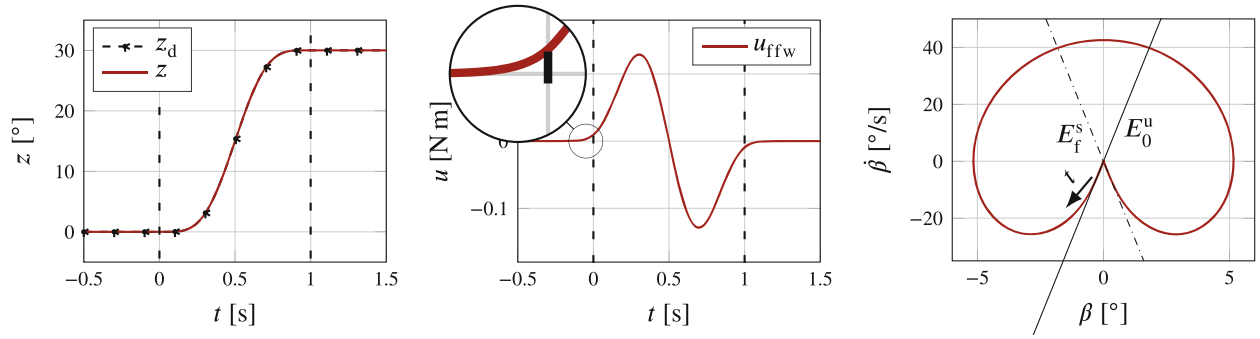

(A) Desired trajectory and simulated system output z. **(B)** Desired system input u_{ffw}. **(C)** Phase space of internal dynamics.

FIGURE 2 Stable inversion results for the manipulator with one passive joint.

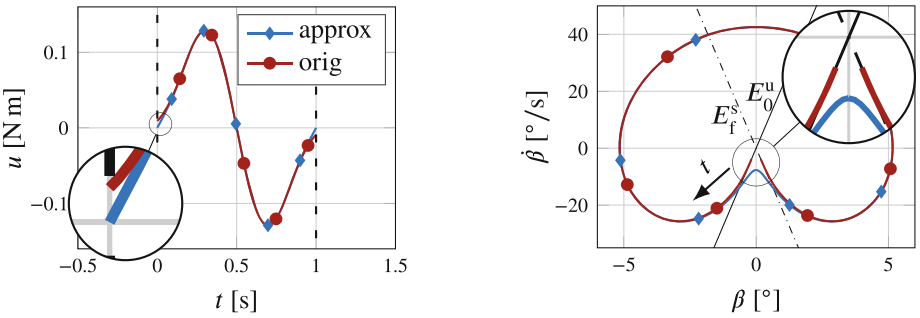

(A) System input u. **(B)** Phase space of internal dynamics.

FIGURE 3 Simulation results for the interval $T_0 = t_0$ and $T_f = t_f$.

In the following, the approximating BVP is compared to the original BVP. The approximated solution is denoted by *approx*, while the original solution is denoted by *orig*. For the approximated boundary conditions, the matrices of Equations (19)–(20) are chosen as

$$\boldsymbol{L}_0^{\mathrm{ode}} = \begin{bmatrix} 1 & 0 \end{bmatrix}, \tag{24}$$

$$\boldsymbol{L}_f^{\mathrm{ode}} = \begin{bmatrix} 1 & 0 \end{bmatrix}. \tag{25}$$

Therefore, the angle β is fixed to the equilibrium point both at the beginning and the end of the trajectory and $\dot{\beta}$ is free. Note that all the other possible boundary conditions, for example, $\boldsymbol{L}_0^{\mathrm{ode}} = \begin{bmatrix} 0 & 1 \end{bmatrix}$ and $\boldsymbol{L}_f^{\mathrm{ode}} = \begin{bmatrix} 1 & 0 \end{bmatrix}$, yield similar solutions.

Figure 3 shows the results for the system input and the phase space for a simulation interval $T_0 = t_0$ and $T_f = t_f$, that is, no allowed pre and postactuation phase. It can be seen that the approximated solution is similar to the original solution over the major part of the trajectory. There are some differences in the beginning of the trajectory due to the approximated boundary condition. Choosing part of the state vector to equal the equilibrium point introduces the error, because the state trajectory cannot start on the unstable manifold. This can be seen in the phase space diagram in Figure 2C in the area around the equilibrium $\beta = 0$.

Increasing the simulation interval, such that $T_0 << t_0$ and $T_f >> t_f$ shows the convergence of the solution. Thereby, the solution interval $[T_0,\ T_f]$ is increased symmetrical around the interval $[t_0,\ t_f]$ with $\Delta T = t_0 - T_0 = T_f - t_f$. The convergence of the system input for larger ΔT is shown in Figure 4A for the input trajectory. For this example, a pre- and postactuation phase of $\Delta T = 0.5$ s is sufficient to recover the solution based on the original boundary conditions. The convergence is shown in terms of the error

$$e(t) = \left\| \boldsymbol{\eta}^{\mathrm{approx}}(t) - \boldsymbol{\eta}^{\mathrm{orig}}(t) \right\| \tag{26}$$

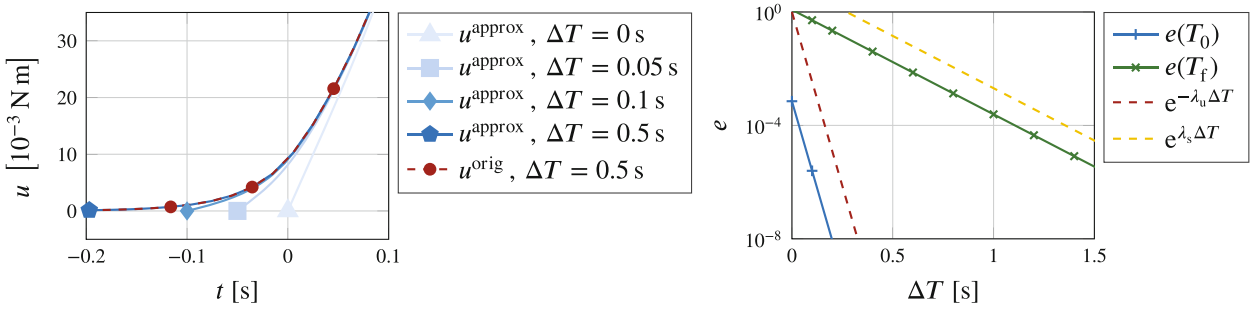

(A) System input u. **(B)** Error e.

FIGURE 4 Convergence of the approximated solution to the correct solution for increasing simulation interval ΔT.

with $\boldsymbol{\eta} = \begin{bmatrix}\beta & \dot{\beta}\end{bmatrix}^{\mathrm{T}}$ in Figure 4B. The logarithmic convergence diagram shows that the error e converges with the speed of the eigenvalue λ_{u} of the internal dynamics at the beginning of the trajectory and with the speed of the eigenvalue λ_{s} at the end of the trajectory. Thereby, λ_{u} and λ_{s} have positive and negative real part respectively, denoting the unstable and stable contributions. Mathematical derivation of the convergence and convergence speed is shown in [11]. Note that in contrast to the previous results, Figure 4B is generated with the damping parameter $d = 0.05\frac{\mathrm{N\,m\,s}}{\mathrm{rad}}$. For this value, the eigenvalues have quite different values and the different convergence speeds at time $T_{=}0$ and T_{f} respectively are visible.

4 | APPLICATION EXAMPLE

For trajectory tracking of highly flexible manipulators, it might not be sufficient to consider only one or two flexible degrees of freedom. Therefore, more complex models should be considered during model inversion. The proposed boundary conditions simplify the application of stable inversion allowing to treat more complex models. As an application example, a flexible manipulator is modeled using the ANCF. The complexity of the equations of motion make an analytical derivation of the internal dynamics burdensome and the original stable inversion formulation is not applicable. The proposed approximation enables the application of stable inversion to the ANCF beams. In the following, the ANCF model is first introduced. Afterwards, simulation results for the approximated stable inversion problem are shown.

4.1 | Flexible manipulator modeled by the ANCF

A flexible manipulator is presented in the following and shown in Figure 5. Equivalently to the manipulator discussed above, a single input u is mounted on the left hand joint and actuates the flexible manipulator. The system output z is the angle between end-effector and the horizontal line. The flexible manipulator is modeled using the absolute nodal coordinate formulation, which is a nonlinear finite element approach. In contrast to classical finite elements, the ANCF accounts for large rigid body rotations [29]. Here, the two-dimensional beam element introduced in [21] is considered. The beam element relaxes Euler-Bernoulli assumptions in the sense that shear deformations are allowed and the beam cross-section does not stay perpendicular to the neutral axis [21]. The undeformed and deformed beam configurations are shown in Figure 6. Thereby, the cross-section coordinate frame describes the orientation of the beam cross-section. The neutral axis coordinate frame describes the orientation of the tangent of the neutral axis.

Following [21], the ANCF beam is briefly introduced. An arbitrary point on a beam element is described by the position vector

$$\boldsymbol{r} = \begin{bmatrix} r_1 \\ r_2 \end{bmatrix} = \boldsymbol{S}(x, y)\, \boldsymbol{e} \tag{27}$$

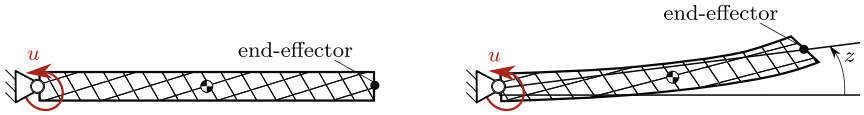

FIGURE 5 Model of a flexible manipulator modeled by the ANCF.

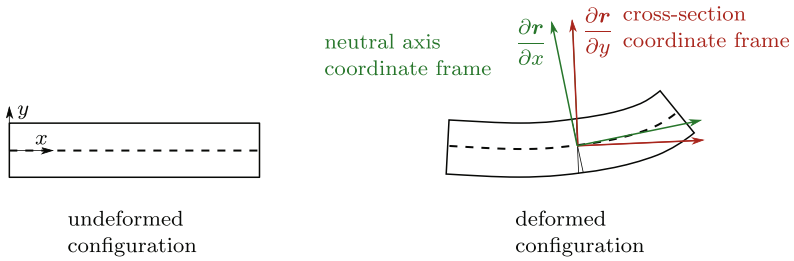

FIGURE 6 Deformed and undeformed configuration of an ANCF element.

with the global element shape function $\boldsymbol{S} \in \mathbb{R}^{2\times 12}$ and the vector of generalized coordinates $\boldsymbol{y} = \boldsymbol{e} \in \mathbb{R}^{12}$. For one ANCF element of length L, the generalized coordinates e_i with $i = 1, 2, \ldots, 6$ at the left node are expressed as

$$e_1 = r_1\Big|_{x=0}, \quad e_2 = r_2\Big|_{x=0}, \tag{28}$$

$$e_3 = \frac{\partial r_1}{\partial x}\Big|_{x=0}, \quad e_4 = \frac{\partial r_2}{\partial x}\Big|_{x=0}, \quad e_5 = \frac{\partial r_1}{\partial y}\Big|_{x=0}, \quad e_6 = \frac{\partial r_2}{\partial y}\Big|_{x=0} \tag{29}$$

and the coordinates e_i with $i = 7, 8, \ldots, 12$ at the right node are

$$e_7 = r_1\Big|_{x=L}, \qquad e_8 = r_2\Big|_{x=L}, \tag{30}$$

$$e_9 = \frac{\partial r_1}{\partial x}\Big|_{x=L}, \quad e_{10} = \frac{\partial r_2}{\partial x}\Big|_{x=L}, \quad e_{11} = \frac{\partial r_1}{\partial y}\Big|_{x=L}, \quad e_{12} = \frac{\partial r_2}{\partial y}\Big|_{x=L}. \tag{31}$$

Thereby, x denotes the undeformed coordinate axis in beam direction with $x \in [0; L]$ and y describes the direction perpendicular to x in the undeformed configuration. For interpolation of the motion, the global shape function matrix is defined as

$$\boldsymbol{S}(x,y) = \begin{bmatrix} s_1(x,y) & 0 & s_2(x,y) & 0 & s_3(x,y) & 0 & s_4(x,y) & 0 & s_5(x,y) & 0 & s_6(x,y) & 0 \\ 0 & s_1(x,y) & 0 & s_2(x,y) & 0 & s_3(x,y) & 0 & s_4(x,y) & 0 & s_5(x,y) & 0 & s_6(x,y) \end{bmatrix}. \tag{32}$$

Thereby, the shape functions are

$$s_1(x,y) = 1 - 3\xi^2 + 2\xi^3, \qquad s_2(x,y) = L\left(\xi - 2\xi^2 + \xi^3\right), \qquad s_3(x,y) = L\left(\eta - \xi\,\eta\right), \tag{33}$$

$$s_4(x,y) = 3\xi^2 - 2\xi^3\,, \qquad s_5(x,y) = L\left(-\xi^2 + L\xi^3\right)\,, \qquad s_6(x,y) = L\xi\,\eta, \tag{34}$$

with $\xi = x/L$ and $\eta = y/L$. The matrices of the equations of motion (2) for one element arise as

$$\boldsymbol{M} = \int_V \rho\, \boldsymbol{S}(x,y)^{\mathrm{T}}\, \boldsymbol{S}(x,y)\, \mathrm{d}V, \tag{35}$$

$$\boldsymbol{k} = \boldsymbol{0}, \tag{36}$$

$$\boldsymbol{q}(\boldsymbol{y}) = -\boldsymbol{K}(\boldsymbol{e})\,\boldsymbol{e} \tag{37}$$

were ρ is the density of the beam, V denotes the volume of one element and $\boldsymbol{K} \in \mathbb{R}^{12\times12}$ is a state dependent stiffness matrix. Note that the mass matrix $\boldsymbol{M}$ is constant over time and is evaluated before the simulation for computational efficiency. The derivation of the elastic forces $\boldsymbol{q}$ is taken from [13], who take a general continuum mechanics approach to model the elastic forces. They arise from the strain energy U_e as

$$\boldsymbol{q}(\boldsymbol{y}, \boldsymbol{v}, t) = \frac{\partial U_e}{\partial \boldsymbol{e}}. \tag{38}$$

Substituting a linear material model for the strain energy U_e and using simplifications shown in [13] yields the simplified elastic forces in the form of Equation (37). Note that using this approach, expensive evaluations of the volume integrals at each time step are avoided. Instead, a few invariant matrices are calculated beforehand to simplify the evaluation of the stiffness matrix $\boldsymbol{K}$. Another advantage of this approach lies in the simple derivation of the Jacobian matrix of the elastic forces, which can be derived completely analytically, see [13] for details. The analytical Jacobian matrices are also relevant for the efficient numerical solution of the large but sparse boundary value problem.

The joint at the left node, see Figure 5, is enforced by the algebraic constraint

$$\boldsymbol{c}_1(\boldsymbol{e}) = \begin{bmatrix} e_1 \\ e_2 \end{bmatrix} = \boldsymbol{0}, \tag{39}$$

and the equations of motion arise in DAE form. The system input u is considered as a velocity-controlled actuator acting on the left node. A zero-order hold model is assumed for the actuator, such that the actuator velocity u equals the rotational velocity $\dot{\gamma}$ of the cross-section at the left joint. Mathematically, this is described by the constraint

$$c_2(\boldsymbol{y}) = u - \dot{\gamma} = u + \frac{e_6\ \dot{e}_5 - e_5\ \dot{e}_6}{e_5^2 + e_6^2} = 0. \tag{40}$$

The system output z is defined as the angle between the right hand node and the horizontal, see Figure 5 with

$$z = \arctan\left(\frac{e_{6(N+1)-4}}{e_{6(N+1)-5}}\right), \tag{41}$$

where N is the number of ANCF beam elements. Note that the considered system output z is not a function of the actuated coordinates. This property and the complex dynamic equations make a direct derivation of the internal dynamics burdensome.

4.2 | Stable inversion results

In the following, stable inversion is applied to the flexible manipulator from Figure 5. The model parameters for the ANCF beam with squared cross-section are given in Table 2. The boundary value problem is setup for the complete inverse model described by servo-constraints considering the approximating boundary conditions (21)–(22). Therefore, the internal dynamics in the coordinates $\boldsymbol{\eta}$ are not derived explicitly. The Simpson scheme is again used for discretization and the step size is chosen as $h = 0.01$ s. The resulting set of nonlinear equations is solved using Newton's method. The initial guess for the boundary value problem is obtained by computing the system input u_{rigid} for an equivalent rigid system and applying it to the flexible system with increased stiffness $E = 1.2 \times 10^9$ Pa in a forward simulation. Alternatively, the initial guess can for example be obtained by redefining the system output to obtain stable internal dynamics and computing the respective inverse model by forward time integration.

For the first model inversion results, a number of $N = 4$ ANCF beam elements are considered in order to limit the computational effort. They yields a number of $6(N + 1) - 3 = 27$ unactuated coordinates. For this system, a number of $12(N + 1) + 4 = 64$ boundary conditions according to Equations (21)–(22) must be specified. As mentioned in Section 3.3, there is a freedom in the choice of simplified boundary conditions. In the simple case of the manipulator with one passive joint, all possible choices yield similar solutions. For the more involved ANCF case, it is an open research question how to define a priori permissible simplified boundary conditions. Some heuristic rules of thumb have been identified so far.

TABLE 2 Overview of simulation parameters for the flexible manipulator.

Material parameter	Value	Geometry parameter	Value
ρ	910 kg/m^3	L	1 m
ν	0	A	0.0081 m^2
E	1.2×10^7 Pa	Shape of cross-section	Squared

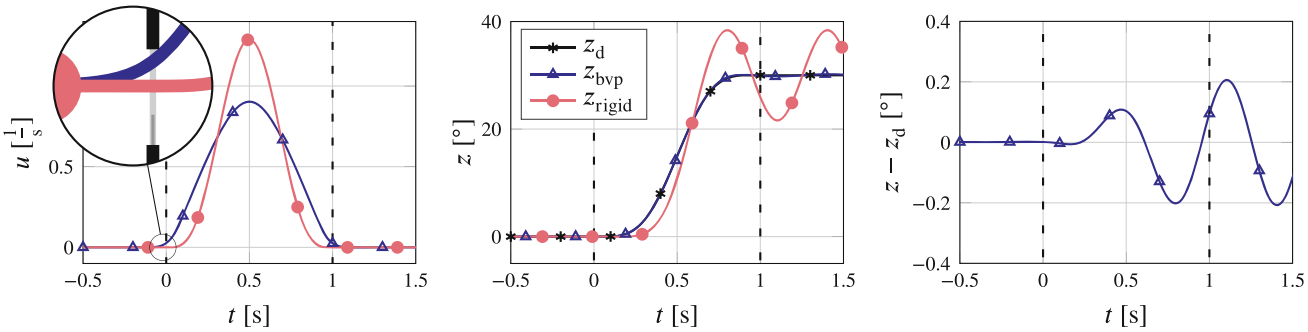

(A) Feedforward input u_{ffw}. **(B)** Simulated system output z. **(C)** Tracking error $e = z - z_{\mathrm{d}}$.

FIGURE 7 Simulation results for stable inversion of four ANCF beam elements.

For the presented example, the following quantities are prescribed at the left (initial) boundary: the slopes relevant for a straight initial configuration, the x and y coordinates of the element nodes, the system input u, the Lagrange multipliers associated with both constraints c_1 and c_2 and some velocities of the generalized coordinates. The following quantities are prescribed at the right (final) boundary: the position of the last node, the system input u, the Lagrange multipliers associated with both constraints c_1 and c_2 and some velocities of the generalized coordinates. There is some freedom especially in the prescription of the initial slopes and the derivatives of the generalized coordinates. For all admissible choices, the numerical results converge to the same results presented above. An analysis for a priori definition of simplified boundary conditions which will yield stable results remains an open research question.

Using the discretization scheme mentioned above, the resulting set of nonlinear equations has the size of $12(N+1)+4 = 64$ unknown coordinates at $\frac{1}{h}(t_{\mathrm{f}} - t_0 + 2\Delta T) + 1$ time instances. For the Simpson discretization in condensed form, algebraic variables must be considered as additional unknown variables at the midpoints of the temporal grid [4]. This yields 4 additional unknowns at $\frac{1}{h}(t_{\mathrm{f}} - t_0 + 2\Delta T)$ time instances. The number of algebraic unknowns is independent of the number of beam elements, since the algebraic variables arise in form of the constraints (39) and (40) and the servo-constraint. For $N = 4$ beam elements solved over the time domain from $T_0 = -1$ s to $T_{\mathrm{f}} = 2$ s, this yields in total a sparse system of 20 464 equations and unknowns.

The system input obtained from the model inversion is then applied to a manipulator modeled by 10 ANCF elements in a forward simulation, since convergence of the ANCF model is reached for approximately 10 elements.

The desired trajectory is chosen as before, see Figure 2A and Equation (23). The results of the stable inversion are shown in Figure 7. They are compared to a simulation with the system input u_{rigid}, which is obtained from inverting an equivalent rigid beam. The system input u_{ffw} obtained from stable inversion features a preactuation phase and differs from the input for the equivalent rigid system, see Figure 7A. This is also reflected in the simulated system output z in Figure 7B. The system input u_{rigid} induces oscillations around the desired final position of approximately 8°, because the flexibility is not accounted for during model inversion. In contrast, the system input from stable inversion of the flexible system captures the dynamics well and yields accurate tracking results in forward simulation. Even though the inversion was performed for only 4 ANCF beam elements, the forward simulation with 10 beam elements shows very accurate tracking. The tracking error $e = z - z_{\mathrm{d}}$ is shown in Figure 7C and has a maximum value of $e = 0.2°$. First of all, the results show that the model inversion with a low number of ANCF elements is reasonable to save computational effort, since the tracking is sufficiently accurate. In contrast, the results demonstrate that inverting the rigid beam is not sufficient for accurate trajectory tracking. In order to visualize the results, the simulation results are shown in x, y-space for different time instances in Figure 8.

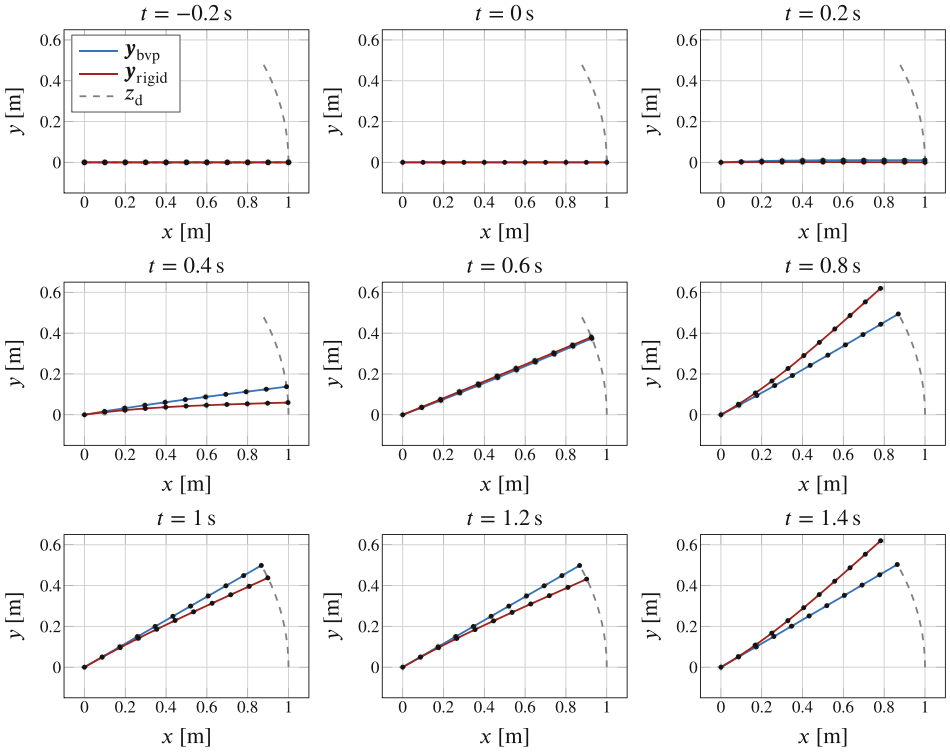

FIGURE 8 Visualization of the motion in space for different time instances.

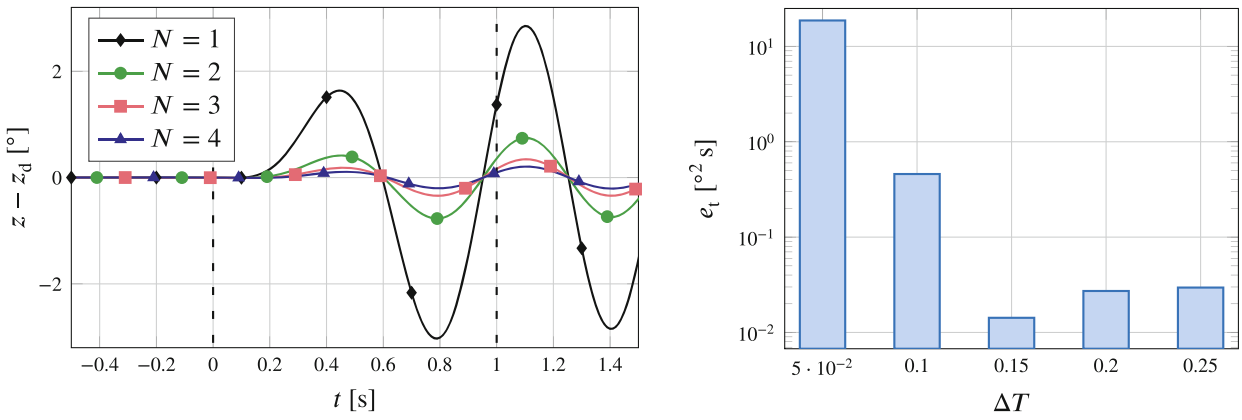

(A) Tracking error $e = z - z_d$ for different number of ANCF elements used in the inverse model.

(B) Cumulated tracking error e_t for different values ΔT.

FIGURE 9 Convergence of the numerical results with respect to number of elements N and with respect to the pre/postactuation time ΔT.

Additionally, the convergence of the inverse model is validated. For this purpose, the inverse model is computed for $N = \{1, 2, 3, 4\}$ ANCF beam elements and the resulting control input is applied to the system with 10 beam elements. The tracking error $z - z_d$ is shown in Figure 9A. The results are computed with a pre/postactuation length $\Delta T = 1$ s. Convergence to a small tracking error is visible. It is postulated that the error completely vanishes for additional elements in the inverse model. However, adding more elements in the inverse model intensifies the numerical difficulties and is not performed here.

Moreover, convergence with respect to the temporal grid is visualized in Figure 9B. Thereby, the value ΔT is varied and the cumulated tracking error e_t of the simulated output z is computed with

$$e_t = \int_{-1\ s}^{2\ s} \|z - z_d\|^2 dt. \tag{42}$$

The forward simulation is again performed with 10 beam elements and 4 ANCF elements are used for model inversion. It can be seen that the tracking error converges for a comparably small value of $\Delta T = 0.2$ s.

5 | SUMMARY

Flexible manipulators arise naturally during the design of lightweight machines. These systems are often underactuated and the trajectory control of such systems is an active field of research. The control is difficult due to the nonminimum phase behavior of many common flexible manipulators. This makes forward integration of the inverse model impossible. Alternatively, the stable inversion approach can be applied. However, the original formulation depends on deriving the internal dynamics explicitly. This is not straightforward for complex multibody systems, such as very flexible manipulators. Therefore, an approximation of the boundary value problem is proposed, which does not rely on deriving the internal dynamics explicitly. It is demonstrated that the approximation converges to the original solution for a simple system with one passive joint. The approximation is then applied to solve the inverse model problem of a highly flexible manipulator, for which it is not possible to determine the internal dynamics. As an application example, the flexible manipulator is modeled using the ANCF. The numerical results show that the proposed approximation yields accurate results for the ANCF model. The results show that superior tracking can be achieved when considering the flexible system during model inversion compared to simply inverting the equivalent rigid system.

ACKNOWLEDGEMENT

This work was supported by the German Research Foundation (Deutsche Forschungsgemeinschaft) via the grant 362536361. Open Access funding enabled and organized by Projekt DEAL.

CONFLICT OF INTEREST STATEMENT

The authors declare that they have no conflict of interest.

REFERENCES

[1] G. Bastos, R. Seifried, and O. Brüls, Inverse dynamics of serial and parallel underactuated multibody systems using a DAE optimal control approach, Multibody Syst Dyn **30** (2013), no. 3, 359–376. https://doi.org/10.1007/s11044-013-9361-z.

[2] G. Bastos, R. Seifried, and O. Brüls, Analysis of stable model inversion methods for constrained underactuated mechanical systems, Mech. Mach. Theory **111** (2017), no. Supplement C, 99–117 http://www.sciencedirect.com/science/article/pii/S0094114X16303135.

[3] T. Berger, The zero dynamics form for nonlinear differential-algebraic systems, IEEE Trans. Automat. Control **62** (2017), no. 8, 4131–4137.

[4] J. Betts, *Practical methods for optimal control and estimation using nonlinear programming*, 2nd ed., Society for Industrial and Applied Mathematics, Philadelphia, PA, 2010. https://doi.org/10.1137/1.9780898718577.

[5] W. Blajer and K. Kołodziejczyk, A geometric approach to solving problems of control constraints: Theory and a DAE framework, Multibody Syst Dyn **11** (2004), no. 4, 343–364.

[6] O. Brüls, G. J. Bastos, and R. Seifried, A stable inversion method for feedforward control of constrained flexible multibody systems, J. Comput. Nonlinear Dyn. **9** (2013), no. 1, 011014–1–011014–9. https://doi.org/10.1115/1.4025476.

[7] M. Burkhardt, R. Seifried, and P. Eberhard, Experimental studies of control concepts for a parallel manipulator with flexible links, J. Mech. Sci. Technol. **29** (2015), no. 7, 2685–2691. https://doi.org/10.1007/s12206-015-0515-1.

[8] D. Chen and B. Paden, Stable inversion of nonlinear non-minimum phase systems, Int. J. Control. **64** (1996), no. 1, 81–97. https://doi.org/10.1080/00207179608921618.

[9] A. De Luca, S. Panzieri and G. Ulivi, Stable inversion control for flexible link manipulators, Proceedings of 1998 IEEE International Conference on Robotics and Automation (Cat. No.98CH36146), Leuven, Belgium, vol. 1, 799–805, 1998.

[10] S. Devasia, D. Chen, and B. Paden, Nonlinear inversion-based output tracking, IEEE Trans. Autom. Control **41** (1996), no. 7, 930–942.

[11] S. Drücker, *Servo-constraints for inversion of underactuated multibody systems*, Phd thesis, Hamburg University of Technology, Hamburg, Germany, 2022. https://doi.org/10.15480/882.4089, http://hdl.handle.net/11420/11463.

[12] J. Escalona, H. Hussien, and A. Shabana, Application of the absolute nodal co-ordinate formulation to multibody system dynamics, J. Sound Vib. **214** (1998), no. 5, 833–851 http://www.sciencedirect.com/science/article/pii/S0022460X98915632.

[13] D. García-Vallejo, J. Mayo, J. L. Escalona, and J. Domínguez, Efficient evaluation of the elastic forces and the jacobian in the absolute nodal coordinate formulation, Nonlinear Dyn **35** (2004), no. 4, 313–329.

[14] K. Graichen, V. Hagenmeyer, and M. Zeitz, A new approach to inversion-based feedforward control design for nonlinear systems, Automatica **41** (2005), no. 12, 2033–2041.
[15] E. Hairer, "*Stiff and differential-algebraic problems*," *Solving ordinary differential equations*, 2nd ed., E. Hairer and G. Wanner (eds.), Springer, Berlin u.a, 2002.
[16] A. Lismonde, V. Sonneville, and O. Brüls, A geometric optimization method for the trajectory planning of flexible manipulators, Multibody Syst. Dyn. **47** (2019), 347–362. https://doi.org/10.1007/s11044-019-09695-z.
[17] L. G. Maqueda, A.-N. A. Mohamed, and A. A. Shabana, Use of general nonlinear material models in beam problems: Application to belts and rubber chains, J. Comput. Nonlinear Dyn. **5** (2010), no. 2, 021003–1–021003–10.
[18] M. Morlock, M. Burkhardt, and R. Seifried, Control concepts for a parallel manipulator with flexible links, Proceedings of Applied Mathematics and Mechanics **16** (2016), no. 1, 819–820.
[19] M. Morlock, N. Meyer, M. A. Pick, and R. Seifried, Real-time trajectory tracking control of a parallel robot with flexible links, Mech. Mach. Theory **158** (2021), 104220 https://www.sciencedirect.com/science/article/pii/S0094114X20304377.
[20] M. Morlock, M. Burkhardt, R. Seifried, and P. Eberhard, End-effector trajectory tracking of flexible link parallel robots using servo constraints, Multibody Syst. Dyn. **56** (2022), 1–28. https://doi.org/10.1007/s11044-022-09836-x.
[21] M. Omar and A. Shabana, A two-dimensional shear deformable beam for large rotation and deformation problems, J. Sound Vib. **243** (2001), no. 3, 565–576.
[22] F. Raouf, S. Mohamad, and S. Maarouf, Workspace tracking control of two-flexible-link manipulator using distributed control strategy, J. Control Sci. Eng. **2013** (2013), 17. https://doi.org/10.1155/2013/617465.
[23] S. Sastry, *Nonlinear systems analysis, stability, and control*, Vol **XXV**, Springer, New York, NY, 1999, 667S.
[24] W. Schiehlen, Applied dynamics*, 215*, Springer International Publishing, Cham s.l., 2014, http://zbmath.org/?q=an:1306.70001.
[25] R. Schwertassek, *Dynamik flexibler Mehrkörpersysteme: Methoden der Mechanik zum rechnergestützten Entwurf und zur Analyse mechatronischer Systeme*, Grundlagen und Fortschritte der Ingenieurwissenschaften, Vieweg, Braunschweig u.a, 1999.
[26] R. Seifried, Integrated mechanical and control design of underactuated multibody systems, Nonlinear Dynamics **67** (2012), no. 2, 1539–1557.
[27] R. Seifried, *Dynamics of underactuated multibody systems modeling, control and optimal design*, Springer International Publishing, Cham, SL, 2014.
[28] A. A. Shabana, Computer implementation of the absolute nodal coordinate formulation for flexible multibody dynamics, Nonlinear Dynamics **16** (1998), no. 3, 293–306. https://doi.org/10.1023/A:1008072517368.
[29] A. A. Shabana, *Dynamics of multibody systems*, 4th ed., Cambridge University Press, Cambridge, 2013. https://doi.org/10.1017/CBO9781107337213.
[30] J.-J. E. Slotine and W. Li, *Applied nonlinear control*, Vol **XV**, Prentice Hall, Englewood Cliffs, NJ, 1991.
[31] T. Ströhle and P. Betsch, A simultaneous space-time discretization approach to the inverse dynamics of geometrically exact strings, Int. J. Numer. Methods Eng. **123** (2022), no. 11, 2573–2609. https://doi.org/10.1002/nme.6951.
[32] H. Sugiyama and Y. Suda, Non-linear elastic ring Tyre model using the absolute nodal coordinate formulation, Proc. Ins. Mech. Eng. K J Multi-Body Dyn. **223** (2009), no. 3, 211–219.
[33] Q. Tian YunQing Zhang, Li-Ping Chen, JingZhou Yang, Two-link flexible manipulator modelling and tip trajectory tracking based on the absolute nodal coordinate method, Proceedings of the 13th National Conference on Mechanisms and Machines (NaCoMM07), 251–258, 2017.
[34] B. Vohar, M. Kegl, and Z. Ren, Implementation of an ANCF beam finite element for dynamic response optimization of elastic manipulators, Eng. Optim. **40** (2008), no. 12, 1137–1150. https://doi.org/10.1080/03052150802317457.

How to cite this article: S. Drücker, and R. Seifried, *Application of stable inversion to flexible manipulators modeled by the absolute nodal coordinate formulation*, GAMM-Mitteilungen. (2023), e202300004. https://doi.org/10.1002/gamm.202300004